INORGANIC CHEMISTRY FRONTIERS

RESEARCH ARTICLE

View Article Online
View Journal | View Issue

Cite this: *Inorg. Chem. Front.*, 2025, **12**, 7820

Revisiting the reported emission spectrum of $Cs_2NaBiCl_6$

Hei-Yui Kai, [a] Daiwen Xiao, [a] Ka-Leung Wong, *[a] Anjun Huang [a,b] and Peter A. Tanner *[a]

Received 10th June 2025,
Accepted 7th August 2025

DOI: 10.1039/d5qi01285f

rsc.li/frontiers-inorganic

In this study, we revisit $Cs_2NaBiCl_6$ and focus upon several assignments previously given for emission bands. A broad emission band spanning from 1200 nm to 1550 nm (centered at ~1350 nm) is observed for Fe^{3+} when excited at 450 nm or shorter wavelengths into its electron transfer bands in chloride double perovskites. This band was previously assigned to a color center (A. Huang, M. Liu, C.-K. Duan, K.-L. Wong and P. A. Tanner, Understanding the Ultraviolet, Green, Red, Near Infrared and Infrared Emission Properties of Bismuth Halide Double Perovskite, *Inorg. Chem. Front.*, 2022, 9, 6379–6390) because it was observed as an unintended impurity in pristine chloride double perovskites. The undoped material also exhibits Cr^{3+} emission which overlaps the 1 μm Bi^{3+} emission. We are unaware of previous reports of Fe^{3+} emission in chloride hosts at an octahedral site. The ms lifetime is typical of $3d^n$–$3d^n$ transitions. This work demonstrates the requirement to check for unintended impurity emission bands from cations at ppm or lower levels.

Introduction

We recently published an understanding of the ultraviolet, green, red, near-infrared and infrared emission properties of a bismuth halide double perovskite (bismuth chloro-elpasolite).[1] With the surge in publications concerning halide double perovskites, we have noticed that many papers have wrongly attributed spectral features because of the presence of unintended impurities. This partly arises from the use of only 99.99% purity rare earth oxides in synthesis, the imperfect synthesis methods which easily produce impurities, and the ease of attack of the final product by moisture. In particular, we have confirmed that the presence of Sb^{3+} impurity has gone unnoticed in many cases.[2] A small amount of metal ion impurity, even at the ppb level, can lead to unwanted emission. It is clear to us that the pristine elpasolites Cs_2NaMCl_6 (M = Y, Lu, La, Sc) do not emit in the visible or infrared spectral regions. For this reason, these transparent compounds have been employed in many studies as hosts for luminescent ions, such as M = Sc for Pr^{3+},[3] Mo^{3+},[4] Cr^{3+},[5–7] V^{3+},[8,9] Er^{3+},[10] and As^{3+}.[11] However, in some other studies, the $Cs_2NaScCl_6$ host is clearly contaminated with Sb^{3+}.[12–14] It was therefore a surprise to read about "dual-band STE emissions encompassing blue and NIR regions" from the $Cs_2NaScCl_6$ host.[15] These are not self-trapped exciton emissions, but rather emissions from the unintentional impurity ions Sb^{3+} [2] and Cr^{3+}.[5–7] It was good news for us to read this paper because it provoked us to re-scrutinize our own assignments in the $Cs_2NaBiCl_6$ study[1] and in this report we revisit some of them.

The optical spectra of Fe^{3+} have been extensively studied in oxide host lattices.[16–18] In particular, the distinction between the spectra of Fe^{3+} at octahedral and tetrahedral sites in oxide systems has been made clear.[19–21] The data are much sparser for halide host lattices. Emission of Fe^{3+} has been assigned in γ-AlF_3 to a broad band at 735 nm.[22] There are broad emission bands at 820 nm in Na_3FeF_6 [23] and at 826 nm in Na_3AlF_6:Fe^{3+}.[24] However, Poirier and Walsh have assigned sharp features near 700 nm in the 2 K and 30 K emission spectra of $KMgF_3$ doped with iron to Fe^{3+} emission.[25]

Due to the position in the nephelauxetic series, the emission of Fe^{3+} in chloride systems is expected to be at longer wavelengths than for fluoride hosts. The broad emission band reported at 566 nm for $CsCdCl_3$:Fe^{3+} [26] is not due to Fe^{3+} and results from Mn^{2+} or other impurities. We are unaware of other reports of the emission spectra of Fe^{3+} in chloride systems. Perhaps such bands may be beyond the normal range of ultraviolet–visible detectors, or alternatively, nonradiative processes dominate in such cases.

The charge transfer bands of halide systems lie at lower energy than those of oxide systems. Taking advantage of this fact, Neuenschwander *et al.* made a careful study of the electron transfer bands in the absorption spectrum of Fe^{3+} doped in the Cs_2NaYCl_6 system, where this ion occupies an octahedral symmetry site with $FeCl_6^{3-}$ coordination (Fig. 1a).[27]

[a]*Department of Applied Biology and Chemical Technology, The Hong Kong Polytechnic University, Hung Hom, Kowloon, Hong Kong S. A. R., P. R. China. E-mail: klgwong@polyu.edu.hk, peter.a.tanner@gmail.com, monkey.tanner@polyu.edu.hk*
[b]*College of Materials Science and Engineering, Kunming University of Science and Technology, Kunming, 650093, P. R. China*

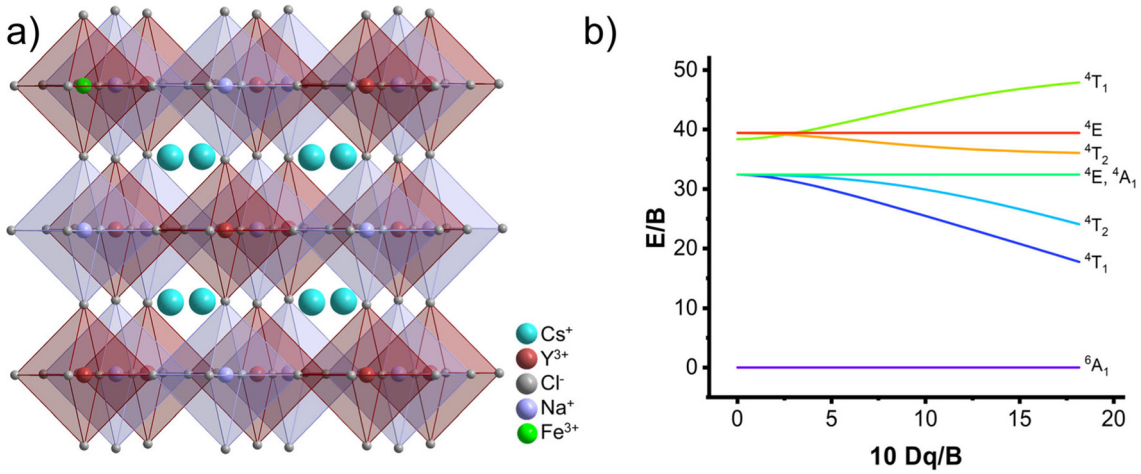

Fig. 1 (a) Structure of Fe^{3+} in Cs_2NaYCl_6. The ionic radii of Y^{3+}(VI) and Fe^{3+}(VI) are 0.9 Å and 0.645 Å, respectively. (b) Schematic Tanabe–Sugano diagram for d^5 ions in octahedral symmetry.

These bands are particularly intense – much more so than the electric dipole and spin forbidden $3d^5$–$3d^5$ intraconfigurational transitions of Fe^{3+}. Hence, they can serve as a fingerprint in the excitation spectra to identify Fe^{3+} in halide double perovskites (elpasolites).

The semiconductor compound $Cs_2NaFeCl_6$ has been well investigated, and it shows strong dependence of the bandgap energy on temperature, giving rise to novel and reversible thermochromic properties. The crystal color changes gradually from light yellow to black in the range of 10–423 K.[28] Armer *et al.* have reported an emission band with a maximum at 517 nm.[29] This band is asymmetric and unusual in that it has a big 'dip' at 534 nm.

Yamatera and Kato[30] published the diffuse reflectance spectra of some $FeCl_6^{3-}$ complexes, with bands at 781 nm and 1124 nm. Xian *et al.*[31] reported a broad band at 750 nm. From these wavelengths, Neuenschwander *et al.*[27] concluded from the Tanabe–Sugano diagram for the d^5 configuration, Fig. 1b, that the Dq/B ratio is near 1.4.

Chen *et al.*[20] attributed the smaller value of the ligand field parameter of Fe^{3+} in octahedral coordination, compared to that of Cr^{3+}, to the reduced effective radius of the 3*d* orbital in the former. These authors have noted that nonradiative quenching of $^4T_1$ Fe^{3+}(oct) luminescence can occur in oxide hosts with $Dq/B \sim 2$ due to crossover with $^2T_2$.

An absorption band at a long wavelength of 1124 nm for the lowest excited state implies that infrared emission is possible. We have therefore investigated the emission spectra for Fe^{3+} in the pristine system $Cs_2NaFeCl_6$ and also for this ion doped into other elpasolite systems. We did not observe infrared emission for $Cs_2NaFeCl_6$ but did observe it for Fe^{3+} doped into other elpasolites. In the course of this work, we discovered that our previous assignment of the infrared emission of $Cs_2NaBiCl_6$ to a color center[1] was incorrect, and it was in fact due to Fe^{3+}.

As mentioned above,[5–7,32] the spectra of Cr^{3+} doped into elpasolite lattices have been thoroughly investigated at low temperatures and high resolution. In contrast to oxide hosts, where the sharp line spin-forbidden $^2E \rightarrow {}^4A_2$ emission bands often appear from unintentional Cr^{3+} impurity, the weaker ligand field choro-elpasolite hosts exhibit broad spin-allowed $^4T_2 \rightarrow {}^4A_2$ emission bands around 1 μm. We detected a weak NIR emission band with several peaks and maximum intensity at ~965 nm for our $Cs_2NaBiCl_6$ samples at room temperature (RT), with the excitation band at 381 nm.[1] This feature was associated with Bi^{3+} at the Cs^+ site. The emission lifetime at 77 K in the region of 900–1000 nm was fitted by biexponential decay with lifetimes of 1 μs and 8 μs. Although the emission is at a similar wavelength to that of Bi^+ doped into various chloride hosts, the moderately intense excitation bands near 600 nm normally associated with Bi^+ are absent and the above lifetimes are much shorter than the 270–765 μs for the chloride hosts.[33] We therefore present alternative evidence that the emission band in $Cs_2NaBiCl_6$ could be due in part to Cr^{3+} impurity.

Luminescence data from recent RT studies of Cr^{3+} doped into elpasolite lattices are summarized in Table 1. The broad emission band around 1 μm is characterized by weak excitation bands near 550 nm and 800 nm, and a stronger band around 300 nm. Interestingly, it was found in the study of $Cs_2(Na,Ag)InCl_6$:Cr,Bi [34] that Cr^{3+} emission can be excited by 365 nm radiation, which populates the Bi^{3+} level. The Cr^{3+} emission lifetime varies considerably in the μs range as shown in Table 1, and it has been discussed and fitted in the study of Cs_2NaMCl_6:Cr (M = Y, In) by Knockenmuss *et al.*[32]

Experimental section

Materials

Cesium chloride (CsCl, 99.999%), bismuth(III) oxide (Bi_2O_3, 99.999%) and yttrium(III) oxide (Y_2O_3, 99.9999%) were purchased from Alfa Aesar. Sodium chloride (NaCl, 99.999%) and mineral oil (nujol oil) were purchased from Sigma Aldrich.

Table 1 Spectroscopic details of Cr^{3+} RT emission in elpasolite lattices

System	λ_{exc} (nm)	λ_{em} (max) (nm)	FWHM (nm)	τ	Ref.
Cs_2NaYCl_6:Cr	310, 553, 770	980	185	18 μs	35
$Cs_2NaScCl_6$:Cr	~300, 550, 790	950	—	μs range	36
$Cs_2(Na,Ag)InCl_6$:Cr,Bi	330, 564, 814	1000	—	—	34
$Cs_2AgInCl_6$:Cr,Er	300–400, 500–650, 730–900	1010	—	12 μs	37
$Cs_2NaScCl_6$:Cr	290, 550, 790	970	153	45–62 μs	38
$Cs_2AgInCl_6$:Cr	353, 565, 800	1010	—	13–18 μs	39
$Cs_2NaScCl_6$:Cr	300, 550, 800	950	162	61 μs	40
$Cs_2NaBiCl_6$	550, 765	971	—	—	1
$Cs_2NaBiCl_6$:Cr	568, 793	979 ± 14	—	101 μs[a]	This work
$Cs_2NaScCl_6$:Cr	285, 569	951	189	59 μs	This work

λ_{em}, λ_{exc} are wavelengths of emission and excitation Cr^{3+} bands; FWHM = full width at half maximum of Cr^{3+} emission band; τ = lifetime of the Cr^{3+} emission band. [a] Measured at 77 K.

Hydrochloric acid (HCl, 37%) was purchased from RCI Labscan. None of the above chemicals were further purified.

Synthesis method

Samples were prepared by the evaporation of solutions of the respective halides and also by the hydrothermal method. For Cs_2NaYCl_6 doped with Fe^{3+}, using the latter method, 2 mmol of CsCl, 0.5 mmol of Y_2O_3, 2 mmol NaCl, and 0.01 mmol of $FeCl_3$ (or 0.005 mol Fe_2O_3) were weighed and dissolved in 10 mL of concentrated hydrochloric acid in a 25 mL Teflon vessel. The vessel was sealed in a steel cup and heated at 180 °C in an oven for 12 h, and then slowly cooled to RT at a rate of 3 °C h^{-1}. Crystals at the bottom of the vessel were washed several times with isopropanol before drying on filter paper at RT. Some crystals were coated with nujol oil for storage. Other hexachloroelpasolite systems were prepared analogously.

Instrumental methods

The X-ray diffraction (XRD) patterns of samples were collected using a Rigaku SmartLab 9 kW – Advance instrument with CuKα radiation (λ = 1.5418 Å). The emission, excitation spectra and lifetime measurements at room temperature were recorded using an Edinburgh FLS1000 spectrometer, with a 450 W xenon lamp as the light source and PMT-900 and PMT-1700 detectors for the visible and NIR regions, respectively. A Fluorolog FL3 instrument was also alternatively employed. The absorption spectra were recorded using an Edinburgh LP980 transient absorption spectrometer at RT using the steady state mode. ICP-MS analysis was performed using an Agilent Technologies 7900 series ICP-MS instrument. The materials for ICP-MS measurements were prepared by dissolving 0.2 g of neat sample in 5 mL of concentrated nitric acid (70%, trace metal basis) or 0.001 g of doped samples in 10 mL of Milli-Q water. 100 μL or 1 mL of the resulting solution was diluted with Milli-Q water to reach the total volume of 10 mL for measurements.

The stated temperatures of 77 K herein and other low temperatures in ref. 1 are very approximate due to the use of powder samples in the copper block. The actual sample temperatures are often much higher due to heating by the excitation source. The near infrared spectra were recorded using an Edinburgh FLS1000 Instrument and a Horiba FL3 Instrument. A calibration check of the instruments using the Nd-YAG laser at 575 nm excitation wavelength gave the same emission at 1054 nm as for a phosphate glass reference sample. The instruments were located in different buildings about 500 m apart. We noticed deviations in some cases of ±25 nm for wavelengths measured around 1 μm using the two instruments at different times which can only be caused by environmental conditions and/or faulty alignment. We have accordingly labeled spectra based on the instrument employed.

Results and discussion

Characterization

The XRD patterns of different host elpasolites are shown in Fig. S1. The patterns agree with the pure cubic phase of elpasolite while small diffraction peaks detected in the sample correspond to CsCl and/or NaCl impurities. ICP-MS analysis was carried out for pristine (Table S1) and Cr/Fe doped elpasolites (Table S2). The concentration of Fe and Cr in pristine $Cs_2NaBiCl_6$ were found to be 169 and 683 ppb, respectively.

Fe^{3+} emission in elpasolites

The low temperature ~1350 nm emission band observed under ~320–460 nm excitation in $Cs_2NaBiCl_6$ (Fig. 2a)[1] is also observed in pristine $Cs_2NaLuCl_6$ [1] and in Fe-doped $Cs_2NaYbCl_6$ (Fig. 2a). The long wavelength side of the emission band is decorated by water absorption. This does not occur for the RT $Cs_2NaY_{0.99}Fe_{0.01}Cl_6$ spectrum (Fig. 2b) and the 77 K spectrum of $Cs_2NaY_{0.99}Fe_{0.1}Cl_6$ (Fig. 2c). The emission band has the maximum wavelength of 1360 ± 40 nm with the full width at half maximum (FWHM) of 330 ± 30 nm at RT and 215 nm at 77 K. The excitation spectrum of this emission does not display bands in the visible spectral region but several bands are observed around 300–450 nm (Fig. 2d(i) and (ii)). The charge transfer absorption bands of Fe^{3+} doped into Cs_2NaYCl_6 in the study of Neuenschwander *et al.*[27] are displayed in Fig. 2d(iii) and show a characteristic fingerprint

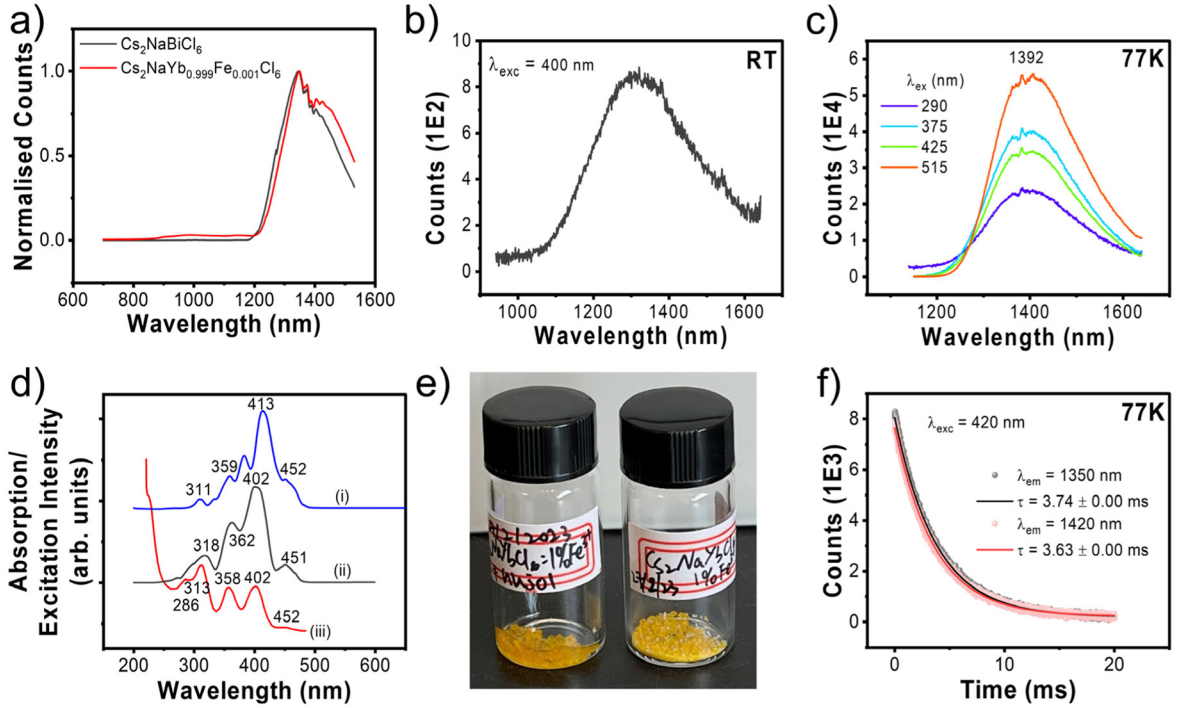

Fig. 2 (a) (black) 400 nm excitation emission spectrum of $Cs_2NaYb_{0.999}Fe_{0.001}Cl_6$:$Fe^{3+}$ at 13 K; (red) 410 nm excitation emission spectrum of $Cs_2NaBiCl_6$ at 10 K. (b) RT $Cs_2NaY_{0.99}Fe_{0.01}Cl_6$ emission spectrum; (c) 77 K emission spectrum of $Cs_2NaY_{0.9}Fe_{0.1}Cl_6$. (d) (i) 10 K excitation spectrum of 1400 nm emission of $Cs_2NaBiCl_6$. (ii) 13 K excitation spectrum of 1346 nm emission of $Cs_2NaYb_{0.99}Fe_{0.01}Cl_6$; (iii) 8 K absorption spectrum of $Cs_2NaY_{0.99}Fe_{0.001}Cl_6$ adapted from ref. 27; the spectra in (a) were recorded using a Horiba FL3 instrument, while the spectra in (b) and (c) were measured using an FLS1000 instrument. (e) Photograph of $Cs_2NaYb_{0.99}Fe_{0.01}Cl_6$ crystals prepared by hydrothermal synthesis with (left) and without (right) nujol. (f) Luminescence decay of Fe^{3+} emission in $Cs_2NaY_{0.99}Fe_{0.01}Cl_6$ at 77 K.

which matches the bands in the excitation spectra of the infrared emission spectra of $Cs_2NaYbCl_6$:Fe^{3+} in Fig. 2d(ii) and pristine $Cs_2NaBiCl_6$ in Fig. 2d(i). The absorption spectra in Fig. S2 exhibit similar features in the region 500–260 nm and show total absorption when the doping concentration of Fe^{3+} is 10%. We consider that this is sufficient proof to show that the infrared emission is due to Fe^{3+}. No other excitation bands are observed because the intensity of the charge transfer transitions is much greater than for $3d^5$–$3d^5$ transitions. The doped $Cs_2NaYbCl_6$ crystals exhibit a yellow color, which is a more pronounced brown in the 1 at% doped material (Fig. 2e). The 77 K luminescence lifetime of the Fe emission in $Cs_2NaY_{0.99}Fe_{0.01}Cl_6$ exhibits monoexponential decay with a lifetime of 3.69(6) ms (Fig. 2f), which increases to 6.0 ms at 40 K. In each case above, the Fe^{3+} ion is envisaged to replace the metal M octahedral symmetry site in Cs_2NaMCl_6 and the $3d^5 \rightarrow 3d^5$ emission corresponds to the $^4T_1 \rightarrow {}^6A_1$ transition.

Cr^{3+} emission in elpasolite lattices

Fig. 3a displays the infrared emission spectra of $Cs_2NaBiCl_6$ published in Fig. 7a of ref. 1. We have assigned the broad feature labeled at 1356 nm to Fe^{3+} emission. The structured band around 1 μm was previously associated with Bi^{3+} at the Cs^+ site. While the latter assignment may be valid, we now recognize that the unusual shape of the band is due in part to the superposition of the spin-allowed $^4T_2 \rightarrow {}^4A_2$ transition of Cr^{3+}. Fig. 3b demonstrates the effect on the emission band of intentionally doping Cr^{3+} into $Cs_2NaBiCl_6$ and using different excitation lines. The 296 nm and 556 nm excitation lines are known, from Table 1, to populate Cr^{3+} energy levels and in these cases the emission band is less structured. Saikia *et al.*[34] have shown that excitation into Bi^{3+} energy levels gives rise to Cr^{3+} emission in addition to that from Bi^{3+} in a Cr^{3+}, Bi^{3+} double-doped elpasolite. This is the case for the other excitation wavelengths in Fig. 3b. In our original report, the excitation spectrum of 1000 nm emission of $Cs_2NaBiCl_6$ (Fig. 7g in ref. 1) exhibited an intense feature at 380 nm, and this band is also present in the excitation spectra of the red emission of $Cs_2NaBiCl_6$, indicating host–guest energy transfer. Notably, when the ordinate scale of Fig. 7g in ref. 1 is expanded, as in Fig. 3c herein, the two characteristic Cr^{3+} absorption bands are observed. Fig. 3d and e clearly demonstrate the distinction in band shape between Cr^{3+} emission and both Bi^{3+} and Cr^{3+} emission near 1 μm.

The RT excitation spectrum of 0.1 at.% Cr^{3+} doped into $Cs_2NaScCl_6$ (Fig. 3g) demonstrates that the visible absorption bands are very weak. However, for 5 at.% doping of Cr^{3+} into $Cs_2NaBiCl_6$ at 77 K, the bands are clearly observed in the excitation spectrum (Fig. 3f).

The RT Cr^{3+} emission in $Cs_2NaSc_{0.999}Cr_{0.001}Cl_6$ is monoexponential with a lifetime of 59 μs (Fig. 3i). On cooling to 77 K,

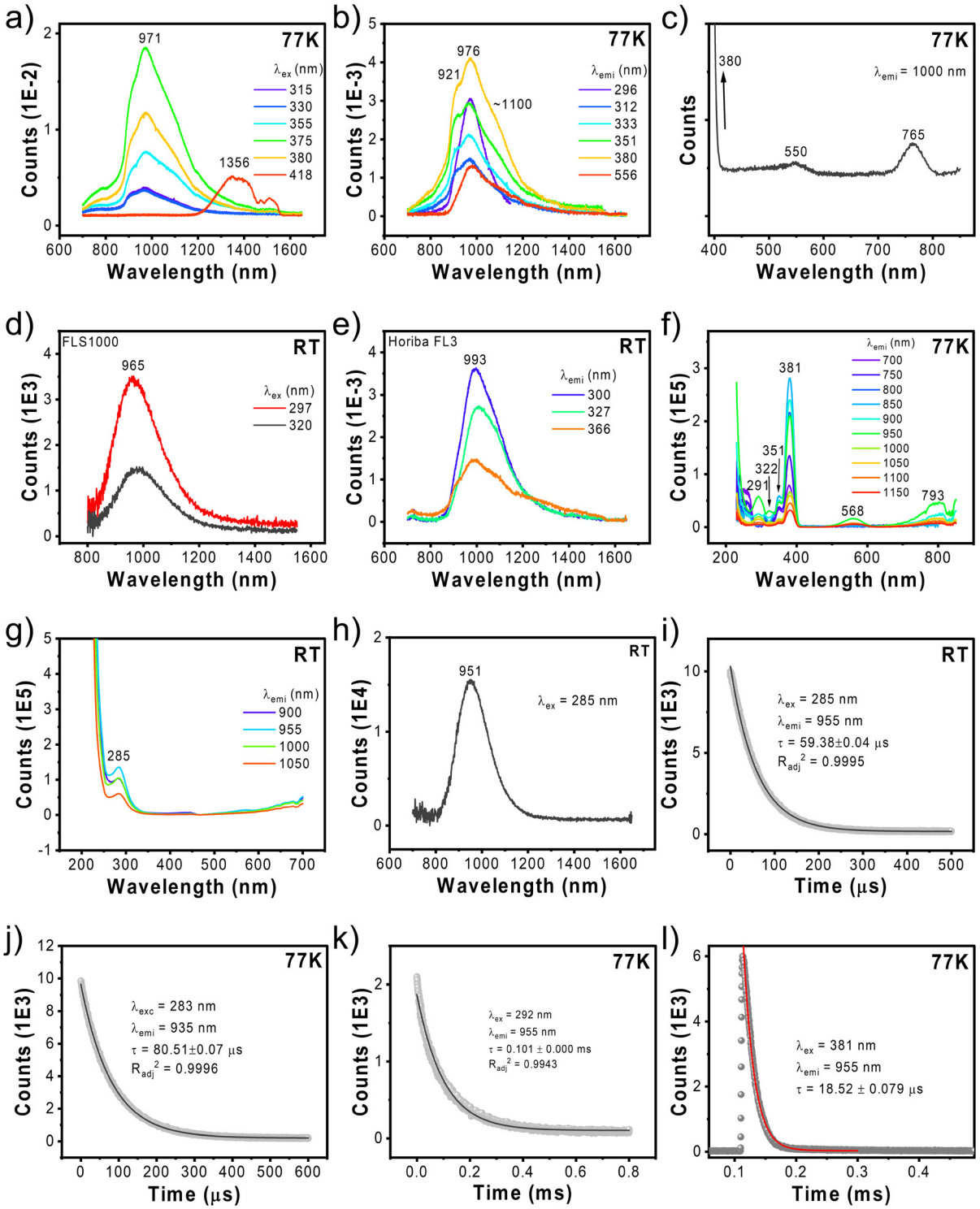

Fig. 3 (a) Reproduced Fig. 7a from ref. 1, showing the 77 K emission spectra of $Cs_2NaBiCl_6$ when using different excitation lines. (b) Nominal 77 K emission spectrum of $Cs_2NaBi_{0.95}Cr_{0.05}Cl_6$ using different excitation lines. (c) Enlarged Fig. 7g from ref. 1 showing part of the 77 K excitation spectrum of the 1000 nm emission of $Cs_2NaBiCl_6$. The weak 550 nm band was not evident in the excitation spectra of 1010 nm or 980 nm emission. Emission spectra of $Cs_2NaBi_{0.95}Cr_{0.05}Cl_6$ recorded using (d) FLS1000 and (e) Horiba FL3, respectively. (f) Excitation spectra of $Cs_2NaBi_{0.95}Cr_{0.05}Cl_6$. (g) Excitation and (h) emission spectra of $Cs_2NaSc_{0.999}Cr_{0.001}Cl_6$. Decay measurements of $Cs_2NaSc_{0.999}Cr_{0.001}Cl_6$ at (i) RT and (j) 77 K, respectively. Lifetimes of $Cs_2NaBi_{0.95}Cr_{0.05}Cl_6$ using (k) 292 nm and (l) 381 nm excitation, respectively.

it increases to 80 μs (Fig. 3j). A value of 101 μs was recorded at 77 K for the Cr^{3+} emission in $Cs_2NaBi_{0.95}Cr_{0.05}Cl_6$ using 292 nm excitation into Cr^{3+} energy levels (Fig. 3k), but a rather lower lifetime of 18 μs is observed when exciting at 381 nm into the Bi^{3+} absorption band (Fig. 3l), which is still longer than in our previous report using 355 nm excitation. The measured lifetime is therefore very sensitive to the excitation wavelength.

Conclusions

The presence of trace impurities at ppm or lower levels can lead to spurious emission bands for elpasolites. We have previously demonstrated this for Sb^{3+} and herein we observe unintended emission from Fe^{3+} and Cr^{3+} in the pristine elpasolite $Cs_2NaBiCl_6$. The previous assignment[1] given for the 1 μm Bi^{3+} emission is deemed valid, but the broad band is overlapped by another from Cr^{3+}. The previous assignment of the 1350 nm infrared emission has been changed to the $^4T_1 \rightarrow {}^6A_1$ transition of Fe^{3+}. The infrared emission of Fe^{3+} complements that known for Cr^{3+} and Ni^{2+} in halide systems.[41]

Conflicts of interest

There are no conflicts to declare.

Data availability

The data in this manuscript will be made available upon reasonable request to the authors.

Supplementary information available: analytical results; X-ray diffractograms; room temperature absorption spectra. See DOI: **https://doi.org/10.1039/d5qi01285f**.

Acknowledgements

K.-L. W acknowledges financial assistance from the Hong Kong Research Grants Council No. 12300021 and NSFC/RGC Joint Research Scheme (N_PolyU209/21).

References

1 A. Huang, M. Liu, C.-K. Duan, K.-L. Wong and P. A. Tanner, Understanding the Ultraviolet, Green, Red, Near Infrared and Infrared Emission Properties of Bismuth Halide Double Perovskite, *Inorg. Chem. Front.*, 2022, **9**, 6379–6390.

2 H.-Y. Kai, D. Xiao, K.-L. Wong, C.-K. Duan and P. A. Tanner, The Importance of Metal Ion Impurity Bands in the Photoluminescence of Halide Double Perovskites, *Adv. Opt. Mater.*, 2025, 2500239.

3 X. J. Zhou, P. A. Tanner and M. D. Faucher, Luminescence of $Cs_2NaScCl_6$:Pr^{3+}: Effects of Changing the Elpasolite Lattice Parameter, *Spectrosc. Lett.*, 2007, **40**, 349–366.

4 C. D. Flint and A. G. Paulusz, Infrared and Visible Luminescence Spectra of $MoCl_6^{3-}$ and $MoBr_6^{3-}$ in Cubic Elpasolite Crystals, *Mol. Phys.*, 1981, **44**, 925–938.

5 O. S. Wenger and H. U. Güdel, Optical Spectroscopy of $CrCl_6^{3-}$ Doped $Cs_2NaScCl_6$: Broadband Near-Infrared Luminescence and Jahn-Teller Effect, *J. Chem. Phys.*, 2001, **114**, 5832–5841.

6 W. StrÈ©k, E. Łukowiak, J. Hanuza, E. Mugenski, R. Cywinski and B. Jeżowska-Trzebiatowska, Fluorescence Properties of Cr^{3+} in the $Cs_2NaScCl_6$ Crystal, *J. Mol. Struct.*, 1984, **115**, 497–500.

7 O. S. Wenger, R. Valiente and H. U. Güdel, Influence of Hydrostatic Pressure on the Jahn–Teller Effect in the $^4T_{2g}$ excited state of $CrCl_6^{3-}$ doped $Cs_2NaScCl_6$, *J. Chem. Phys.*, 2001, **115**, 3819–3826.

8 C. Reinhard, K. Krämer, D. A. Biner and H. U. Güdel, V3+ Sensitized Upconversion in $Cs_2NaScCl_6$:Pr^{3+};V^{3+} and K_2NaScF_6:Er^{3+};V^{3+}, *J. Alloys Compd.*, 2004, **374**, 133–136.

9 C. Reinhard and H. U. Güdel, Cooperative Processes in Pr^{3+} and V^{3+} Codoped $Cs_2NaScCl_6$, *J. Lumin.*, 2003, **102–103**, 373–379.

10 C. Zhao, Y. Gao, T. Song, J. Wang and J. Qiu, An Er^{3+}-Doped $Cs_2NaScCl_6$ Lead-Free Double Perovskite with Efficient Broadband Visible to Near-Infrared Emission and Multimodal Upconversion Luminescence, *J. Phys. Chem. Lett.*, 2023, **14**, 9011–9018.

11 E. W. J. L. Oomen, W. M. A. Smit and G. Blasse, The Luminescence of Arsenic(III) in the Cubic Elpasolite $Cs_2NaScCl_6$, *Chem. Phys. Lett.*, 1987, **138**, 584–586.

12 Y. Li, Q. Luo, X. Huang, H. Lu, Y. Yuan, X. Xu, S. Wang and S. Wu, Red-Emitting $Cs_2NaScCl_6$:Sm Flexible Films for High-Resolution X-Ray Imaging, *CrystEngComm*, 2024, **26**, 2404–2412.

13 G. Yang, S. Bai, X. Li, H. Liang, C. Li, J. Sun, Y. Wang, J. Huang, G. Pan and Y. Zhu, Tunable and Efficient Photoluminescence of Lanthanide-Doped $Cs_2NaScCl_6$ Double Perovskite Single Crystals toward Multifunctional Light-Emitting Diode Applications, *ACS Appl. Mater. Interfaces*, 2023, **15**, 24629–24637.

14 R. Zhang, Z. Wang, X. Xu, X. Mao, J. Xiong, Y. Yang and K. Han, All-Inorganic Rare-Earth Halide Double Perovskite Single Crystals with Highly Efficient Photoluminescence, *Adv. Opt. Mater.*, 2021, **9**, 2100689.

15 Y. Liu, D. Tu, M. Yang, H. Li, C. Li, Z. Xie, S. Zhou, S. Yu, J. Xu and X. Chen, Near-Infrared and Visible Dual-Band Self-Trapped Exciton Emissions from Li^+-Doped $Cs_2NaScCl_6$ Double Perovskites, *ACS Energy Lett.*, 2025, **10**, 2150–2159.

16 K. Kniec, W. Piotrowski, K. Ledwa, L. D. Carlos and L. Marciniak, Spectral and Thermometric Properties Altering Through Crystal Field Strength Modification and Host Material Composition in Luminescence Thermometers Based on Fe^{3+} doped AB_2O_4 Type

Nanocrystals (A = Mg, Ca; B = Al, Ga), *J. Mater. Chem. C*, 2021, **9**, 517–527.
17 M. Mrad, A. Tarhini and V. Giordano, Absorbance and Energy Levels for a Fe^{3+} ion in α-Al_2O_3. Optical Pumping Applied to a 31 GHz Maser, *Curr. Appl. Phys.*, 2020, **20**, 1366–1372.
18 A. Novatski, A. Somer, F. G. Maranha, E. C. F. de Souza, A. V. C. Andrade, S. R. M. Antunes, C. P. F. Borges, D. T. Dias, A. N. Medina and N. G. C. Astrath, Effect of Magnetic Coupling on Non-Radiative Relaxation Time of Fe^{3+} Sites on $LaAl_{1-x}Fe_xO_3$ pigments, *J. Appl. Phys.*, 2018, **123**, 075101.
19 Q. Chen, C. Ji and C.-K. Duan, Luminescence of Iiron Ions in Crystals: Site Occupancy, Valence States, and Excited-State Properties, *Phys. Rev. B*, 2024, **109**, 165124.
20 Q. Chen, Q. Quan and C.-K. Duan, Uncovering the Presence or Absence of Photoluminescence from Iron Ions in Crystals, *Phys. Rev. Mater.*, 2024, **8**, 095201.
21 Y. Wang, A. Chen, S. Jiang, L. Zhong, L. Li, X. Zhou, C.-K. Duan and Q. Chen, Theoretical Design and Experimental Realization of Fe^{3+}-Doped Dual-Band Near-Infrared Garnet Phosphors, *Inorg. Chem. Front.*, 2025, **12**, 1383–1392.
22 D. J. Telfer and G. Walker, Fe^{3+} Luminescence Centres in Aluminium Fluoride, *J. Lumin.*, 1976, **11**, 315–320.
23 F. He, E. Song, C. Zhang, H. Chang, G. Dong, Z. Xia, W. Wang and Q. Zhang, Cr^{3+}↔Fe^{3+} Energy Transfer Offset Enabling Anti-Thermal Quenching Near-Infrared Emission for Coded Wireless-Communication Applications, *Laser Photonics Rev.*, 2024, **18**, 2300668.
24 F. Q. He, E. H. Song and Q. Y. Zhang, Energy Transfer-Induced Blue Light-Excited Broadband Near-Infrared Luminescence in Fluoride Na_3AlF_6:Mn^{4+},Fe^{3+}, *J. Mater. Chem. C*, 2024, **12**, 15137–15143.
25 A. Poirier and D. Walsh, Photoluminescence of Iron-Doped $KMgF_3$, *J. Phys. C: Solid State Phys.*, 1983, **16**, 2619.
26 S. Ge, Q. Wei, W. Jia, Y. Liang, C. Peng, Y. Tian and B. Zou, Strong Yellow Emission of Polaronic Magnetic Exciton in Fe^{3+}-doped $CsCdCl_3$ Perovskites, *Appl. Phys. Lett.*, 2021, **118**, 152102.
27 K. Neuenschwander, H. U. Guedel, J. C. Collingwood and P. N. Schatz, Electron-Transfer Transitions in Hexachloroferrate(III). Single-Crystal Absorption and MCD Spectra, *Inorg. Chem.*, 1983, **22**, 1712–1718.
28 F. Ji, J. Klarbring, B. Zhang, F. Wang, L. Wang, X. Miao, W. Ning, M. Zhang, X. Cai, B. Bakhit, M. Magnuson, X. Ren, L. Sun, M. Fahlman, I. A. Buyanova, W. M. Chen, S. I. Simak, I. A. Abrikosov and F. Gao, Remarkable Thermochromism in the Double Perovskite $Cs_2NaFeCl_6$, *Adv. Opt. Mater.*, 2024, **12**, 2301102.
29 M. Armer, P. Dörflinger, A. Weis, C. Büchner, A. Gottscholl, J. Höcker, K. Frank, L. Nusser, M. T. Sirtl, B. Nickel, T. Bein and V. Dyakonov, Low Temperature Optical Properties of Novel Lead-Free $Cs_2NaFeCl_6$ Perovskite Single Crystals, *Adv. Photonics Res.*, 2023, **4**, 2300017.
30 H. Yamatera and A. Kato, The d-d Bands of Hexachloroferrate (III) Ion, *Bull. Chem. Soc. Jpn.*, 1968, **41**, 2220–2220.
31 Y. Xian, H. Yin, Y. Bao, Y. Xiao, S. Yuan, N. U. Rahman, Y. Yuan, Y. Zhang, X. Meng, S. Jin, W. Li and J. Fan, Engineered Electronic Structure and Carrier Dynamics in Emerging $Cs_2Ag_xNa_{1-x}FeCl_6$ Perovskite Single Crystals, *J. Phys. Chem. Lett.*, 2020, **11**, 9535–9542.
32 R. Knochenmuss, C. Reber, M. V. Rajasekharan and H. U. Güdel, Broadband Near–Infrared Luminescence of Cr^{3+} in the elpasolite lattices $Cs_2NaInCl_6$, Cs_2NaYCl_6, and Cs_2NaYBr_6, *J. Chem. Phys.*, 1986, **85**, 4280–4289.
33 D. N. Vtyurina, A. N. Romanov, A. A. Veber, Z. T. Fattakhova, A. A. Antonov, V. B. Tsvetkov and V. N. Korchak, The Spectral Properties and the NIR Photoluminescence of Univalent Bismuth Bi^+ in $RbAlCl_4$, $CsAlCl_4$, $RbMgCl_3$, $CsMgCl_3$, $KCdCl_3$ and $RbCdCl_3$ Crystal Phases, *Russ. J. Phys. Chem. B*, 2016, **10**, 388–393.
34 S. Saikia, A. Ghosh and A. Nag, Broad Dual Emission by Codoping Cr^{3+} (d→d) and Bi^{3+} (s→p) in $Cs_2Ag_{0.6}Na_{0.4}InCl_6$ Double Perovskite, *Angew. Chem., Int. Ed.*, 2023, **62**, e202307689.
35 F. Zhu, Y. Gao, C. Zhao, J. Pi and J. Qiu, Achieving Broadband NIR-I to NIR-II Emission in an All-Inorganic Halide Double-Perovskite Cs_2NaYCl_6:Cr^{3+} Phosphor for Night Vision Imaging, *ACS Appl. Mater. Interfaces*, 2023, **15**, 39550–39558.
36 Z. Wang, Y. Chen, J. Ke, Y. Wei, Y. Liu and M. Hong, Achieving Ultra-Broadband Near-Infrared Emission in Cr^{3+}-Activated $Cs_2NaScCl_6$ Perovskite for Efficient Phosphor-Converted Light-Emitting Diodes, *Adv. Opt. Mater.*, 2024, **12**, 2301323.
37 W. Gan, L. Cao, S. Gu, H. Lian, Z. Xia and J. Wang, Broad-Band Sensitization in Cr^{3+}–Er^{3+} Co-Doped $Cs_2AgInCl_6$ Double Perovskites with 1.5 μm Near-Infrared Emission, *Chem. Mater.*, 2023, **35**, 5291–5299.
38 W. Huang, H. Peng, J. Huang, Y. Yang, Q. Wei, B. Ke, M. S. Khan, J. Zhao and B. Zou, Efficient Near-Infrared Emission in Lanthanum Ion Doped Double Perovskite $Cs_2NaScCl_6$ via Cr^{3+} Sensitization Under Visible Light Excitation, *EcoMat*, 2024, **6**, e12437.
39 F. Zhao, Z. Song, J. Zhao and Q. Liu, Double Perovskite $Cs_2AgInCl_6$:Cr^{3+}: Broadband and Near-Infrared Luminescent Materials, *Inorg. Chem. Front.*, 2019, **6**, 3621–3628.
40 C. Zhao, Y. Gao, J. Wang and J. Qiu, Achieving Nearly Quantitative (~100%) IQE and 42.3% EQE Across NIR-I and NIR-II Regions with Cr^{3+}-doped $Cs_2NaScCl_6$ under 300 nm Excitation, *Laser Photonics Rev.*, 2024, **18**, 2300952.
41 D. Liu, P. Dang, G. Zhang, H. Lian, G. Li and J. Lin, Near-Infrared Emitting Metal Halide Materials: Luminescence Design and Applications, *InfoMat*, 2024, **6**, e12542.

